NANO LETTERS

pubs.acs.org/NanoLett

In Situ TEM Observation of Heterogeneous Phase Transition of a Constrained Single-Crystalline Ag_2Te Nanowire

Juneho In,[†] Youngdong Yoo,[†] Jin-Gyu Kim,[‡] Kwanyong Seo,[†] Hyunju Kim,[†] Hyotchel Ihee,[†] Sang Ho Oh,*[,‡,§] and Bongsoo Kim*[,†]

[†]Department of Chemistry, KAIST, Daejeon 305-701, Korea, [‡]Division of Electron Microscopic Research, KBSI, Daejeon 305-333, Korea, and [§]Department of Material Science and Engineering, POSTECH, Pohang 790-784, Korea

ABSTRACT Laterally epitaxial single crystalline Ag_2Te nanowires (NWs) are synthesized on sapphire substrates by the vapor transport method. We observed the phase transitions of these Ag_2Te NWs via in situ transmission electron microscopy (TEM) after covering them with Pt layers. The constrained NW shows phase transition from monoclinic to a body-centered cubic (bcc) structure near the interfaces, which is ascribed to the thermal stress caused by differences in the thermal expansion coefficients. Furthermore, we observed the nucleation and growth of bcc phase penetrating into the face-centered cubic matrix at 200 °C by high-resolution TEM in real time. Our results would provide valuable insight into how compressive stresses imposed by overlayers affect behaviors of nanodevices.

KEYWORDS Ag_2Te nanowire, phase transitions, in situ TEM, compressive stress, epitaxial growth

Silver telluride (Ag_2Te) is an attractive material that exhibits thermoelectricity, structural phase transitions, and magnetoresistance (MR). Monoclinic Ag_2Te at room temperature (RT) is a narrow band gap semiconductor with high electron mobility and low-lattice thermal conductivity.[1−3] The monoclinic Ag_2Te phase transits to face-centered cubic (fcc) and body-centered cubic (bcc) phases at 145 and 802 °C, respectively, accompanied by changes of electrical resistance and lattice volume.[4−7] Slight change of the stoichiometry of Ag_2Te can induce remarkable MR change at RT.[8,9] These interesting physical properties make Ag_2Te a good candidate for thermoelectric devices, semiconductor switches, and magnetic sensors.

Phase transitions of single-crystalline Ag_2Te nanostructures have been studied with X-ray diffraction (XRD), electrical resistance change, and thermal analysis.[1−3,14,15] Note that significant volume contraction accompanying the phase transition from fcc to bcc makes internal pressure an important variable in the phase transformations of Ag_2Te NW in addition to temperature.[7] In particular, for practical application in nanodevices, it is important to understand how external stresses imposed on the materials affect their phase change performance. It has been reported that substrates and cladding layers surrounding multiphase thin films and NWs can influence their phase transition behaviors as the dimensions of devices are reduced to nanoscale.[12,13]

We have grown epitaxial Ag_2Te NWs horizontally on a sapphire substrate, and also obtained freestanding Ag_2Te NWs in other growth conditions. We have investigated heterogeneous phase transitions of constrained single-crystalline Ag_2Te NWs covered by Pt overlayers on a sapphire substrate using in situ transmission electron microscopy (TEM). Owing to the compressive stress imposed by differences in thermal expansion coefficients between Ag_2Te and sapphire and also Ag_2Te and Pt at elevated temperatures, constrained Ag_2Te NWs show quite distinct phase transition behaviors from the reversible phase change of bulk Ag_2Te. A finite element analysis predicts that large compressive stress is generated near the interfaces of a constrained NW, leading to phase transitions from monoclinic to a bcc structure at the interfaces to relieve this stress, rather than to a fcc structure as in the case of freestanding NWs.

Figure 1a,b shows field emission scanning electron microscopy (FE-SEM) images of Ag_2Te NWs grown on a c-cut

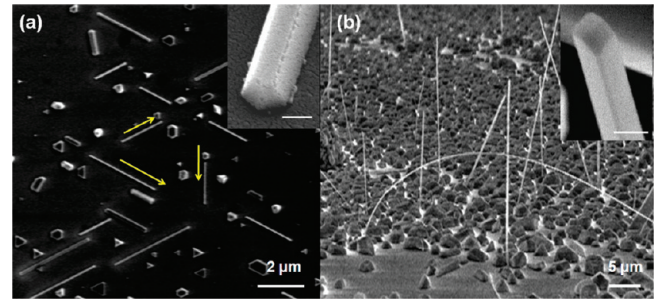

FIGURE 1. FE-SEM images of (a) epitaxial and (b) freestanding growth of Ag_2Te NWs on the c-cut sapphire substrate. Insets display the NWs have well-faceted surfaces at the tip and side. (Inset bar: 100 nm).

* To whom correspondence should be addressed. Fax: +82-42-350-2810. E-mail: (B.K.) bongsoo@kaist.ac.kr; (S.H.O.)shoh@postech.ac.kr.

Received for review: 07/6/2010
Published on Web: 10/12/2010

DOI: 10.1021/nl102350j | *Nano Lett.* **2010,** *10,* 4501–4504

sapphire substrate. The NWs were synthesized in a horizontal quartz tube furnace using Ag_2Te powder (0.01 g, Sigma-Aldrich) as a precursor, which was heated to 980 °C for a reaction time of 30 min. Sapphire substrates were placed ~12 cm from the precursor (see scheme S1 in the Supporting Information). No catalyst was employed. The growth of Ag_2Te NWs was greatly affected by the flow rate of Ar carrier gas. When the Ar flow rate was 25 sccm with a total pressure of 10 Torr, Ag_2Te NWs grow along three equivalent $<10\bar{1}0>$ directions of sapphire, each of which is rotated by 120° on the basal c-plane (Figure 1a). This orientation matches well with the 3-fold symmetry of c-cut sapphire and is identical to those observed for Au and VO_2 NWs grown on c-cut sapphire.[14,15] As Ar flow rate was increased to 50 sccm at the same total pressure of 10 Torr, freestanding Ag_2Te NWs were synthesized after Ag_2Te nanoparticles formed initially (Figure 1b). The Ag_2Te NWs have diameters of 50−150 nm and lengths from a few to tens of micrometers. The NWs are well-faceted at the tip and sidewalls (insets in Figure 1a,b). The diffraction peaks in the XRD patterns of epitaxially grown and freestanding NWs (Supporting Information Figure S1) can be indexed to the standard monoclinic Ag_2Te phase (JCPDS file, 81-1985, $a = 8.164$ Å, $b = 4.468$ Å, $c = 8.977$ Å; space group, $P2_1/c$).

An in situ TEM experiment was performed first with freestanding Ag_2Te NWs, which were separated from the substrate through sonication, dispersed in methanol, and then supported on a TEM grid. The phase transitions of these NWs were investigated in selected area electron diffraction (SAED) modes on a TEM (EM 912Ω) operated at 120 kV. The SAED patterns were obtained from 120 to 170 °C at an increment of 10 °C and also at 175 and 180 °C after waiting 30 min at each temperature with a heating rate of 5 °C/min. Phase transitions of the NWs during the heating−cooling cycle were monitored by observing the change of SAED patterns at the region indicated by a blue circle in Figure 2a. Figure 2b shows that the NW is single crystalline at RT with a growth direction of $[010]_M$ ("M" denotes monoclinic.). The diffraction pattern is indexed to the $[100]_M$ zone pattern of monoclinic Ag_2Te, which started to change phase from 170 °C upon heating (Figure 2c); for example, the intensities of $(h00)_M$ and $(0l0)_M$ spots (h and l are odd integers), the reflections forbidden in an fcc structure, decreased gradually, and some of the high index diffraction spots (e.g., the $(310)_M$ spot) were split (see Supporting Information, Figure S2), indicating the beginning of a phase transition to the fcc phase. At 175 °C, all spots that originated from the monoclinic structure (enclosed only by a circle) disappeared, while some high index diffraction spots (enclosed by both a circle and a square) remained split (Figure 2d). The SAED was indexed to the $[0\bar{1}1]_{fcc}$ zone axis pattern, which was previously the $[001]_M$ zone axis pattern. Transition to the fcc structure was completed at 180 °C. Upon cooling, the fcc phase returned to the monoclinic phase at a temperature slightly below 130 °C (Supporting Information Figure S3).

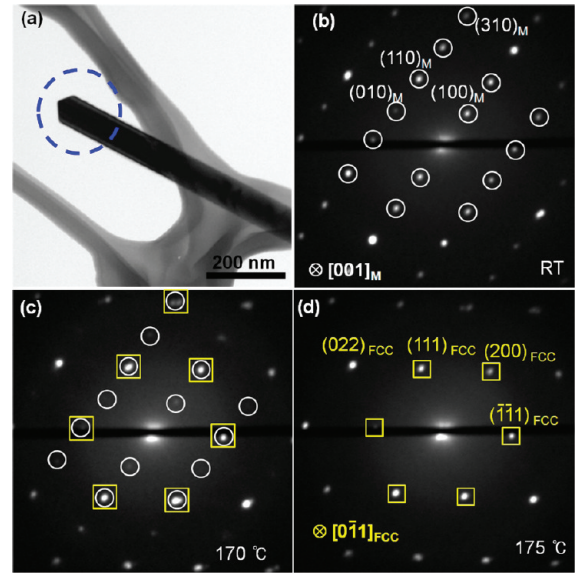

FIGURE 2. In situ SAED patterns of a freestanding Ag_2Te NW obtained from the circle in (a) the bright-field TEM image on a heating−cooling cycle. (b−d) SAED patterns obtained during heating at temperatures of (b) RT; (c) 170 °C; (d) 175 °C (M, monoclinic; white circle, monoclinic spot; yellow square, fcc spot).

Such heating−cooling hysteresis in phase transitions has been observed in other studies.[1−3,10,11]

To investigate the phase transition of a constrained Ag_2Te NW, we prepared epitaxially grown NWs into a cross-sectional lamella using a focused ion beam (FIB). Figure 3a shows a cross-sectional HRTEM image of a monoclinic Ag_2Te NW epitaxially grown on a c-cut sapphire. The NW has a trapezoidal cross-section bounded by the $(001)_M$ top and bottom faces and the $(11\bar{2})_M$ and the $(110)_M$ side facets. Figure 3b shows that the orientation relationship between the Ag_2Te NW and the sapphire substrate is $(110)_M \| (10\bar{1}1)_{sapphire}$. The lattice mismatch between the $(110)_M$ plane of Ag_2Te and the $(10\bar{1}1)$ plane of c-cut sapphire is ~2.3%. The fast Fourier transformation (FFT) patterns of the HRTEM image (Supporting Information Figure S4) correspond to the $[1\bar{1}0]_M$ and $[01\bar{1}0]_{sapphire}$ patterns, respectively, indicating that the NW growth direction is the $[1\bar{1}0]$ direction, which is parallel to the in-plane $[01\bar{1}0]$ direction of c-cut sapphire.

In this FIB-prepared TEM sample (Supporting Information Figure S5), Ag_2Te NWs are covered by two Pt layers, which provide surface protection of the Ag_2Te NWs from redeposition of removed materials. Investigating the stress-induced phase transitions of Ag_2Te NWs sandwiched with cladding layers and substrates would provide insight for employing them in practical device applications as well as help us to understand fundamental phase change performances.[12,13] The thermal expansion of these constrained Ag_2Te NWs is suppressed by the Pt layer and the sapphire substrate, imposing compressive stress on the NW. The thermal stress acting on the Ag_2Te NW at elevated temperatures was calculated by a finite element analysis, using the thermal

DOI: 10.1021/nl102350j | *Nano Lett.* **2010,** *10,* 4501–4504

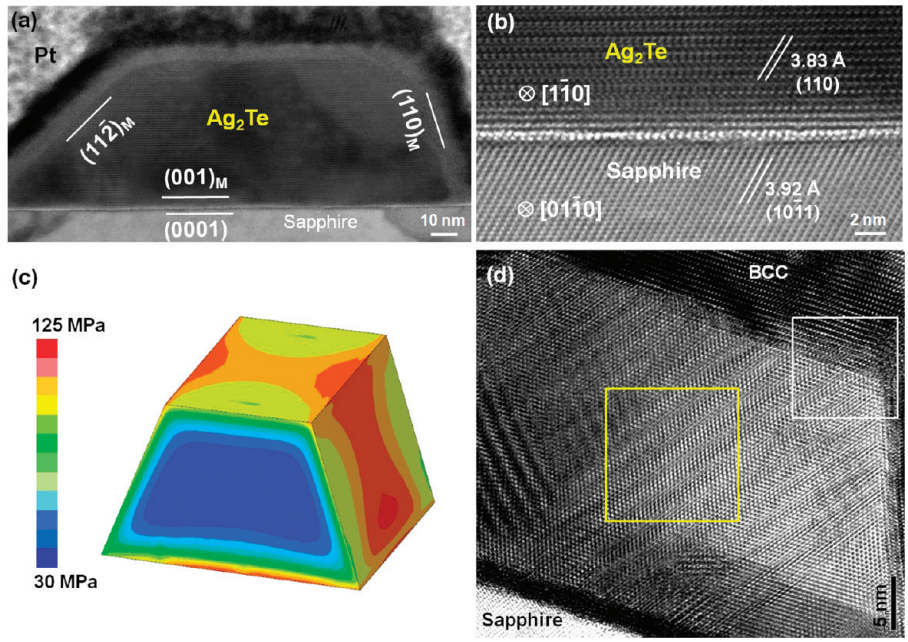

FIGURE 3. (a) Cross-section HRTEM image of epitaxially grown Ag_2Te NW showing a trapezoid cross-section with the (001) top and bottom surfaces and $(110)_M$ and $(11\bar{2})_M$ side facets. (M, monoclinic; S, sapphire). (b) Magnified HRTEM image of the clear interface between sapphire substrate and Ag_2Te NW. (c) Finite element analysis of compressive stress generated at the cross-section of an Ag_2Te NW at 160 °C. The color map is a plot of the pressure of the interface and interior in the NW. It indicates the blue color is ~30 MPa and the dark red is ~125 MPa. (d) Representative cross-section HRTEM image of the epitaxially grown Ag_2Te NW at 150 °C showing the bcc phase at the dark region and wavelike Moiré fringes at the bright region.

expansion coefficients (α), the mechanical properties (Young's modulus, E and Poisson's ratio, ν) of Ag_2Te ($\alpha = 2 \times 10^{-5}$ K^{-1}, $E \sim 40$ GPa, $\nu \sim 0.3$), sapphire ($\alpha = 8.5 \times 10^{-6}$ K^{-1}, $E = 168$ GPa, $\nu \sim 0.38$), and Pt ($\alpha = 8.8 \times 10^{-6}$ K^{-1}, $E = 345$ GPa, $\nu \sim 0.25$) and the geometry of the sample.[16,17] Figure 3c shows that at 160 °C, for example, the Ag_2Te NW is under compressive stress, which is maximal (~125 MPa) along the boundaries and decreases toward the interior (~30 MPa). Although the calculated stress level is much lower than the hydrostatic pressure predicted for the stabilization of bulk bcc phase by a molecular simulation, ~5 GPa at 523 K, these biaxial compressive stresses, combined with the small loading area and the large surface-to-volume ratio at a nanometer scale, could induce significant pressure effects in the phase transition of the constrained Ag_2Te NW.[7,12,13] In situ TEM investigation of a constrained Ag_2Te NW was carried out using a JEM-ARM 1300S operated at 1250 kV in high-resolution TEM (HRTEM) imaging mode. At around 130 °C, we observed that the monoclinic phase transited to a high-temperature bcc phase preferentially along the boundaries of NWs where the compressive stress is relatively high. Surrounded by this bcc phase, the internal monoclinic phase gradually transformed to fcc phase at higher temperatures. Figure 3d is a snapshot HRTEM image showing these heterogeneous phase transitions at 150 °C. The boundary regions showing dark contrast correspond to the phase-transformed bcc phase (details are shown in Figure 4e,f and Supporting Information Figure S7.). The inside region surrounded by the bcc phase exhibits undulating Moiré fringes,

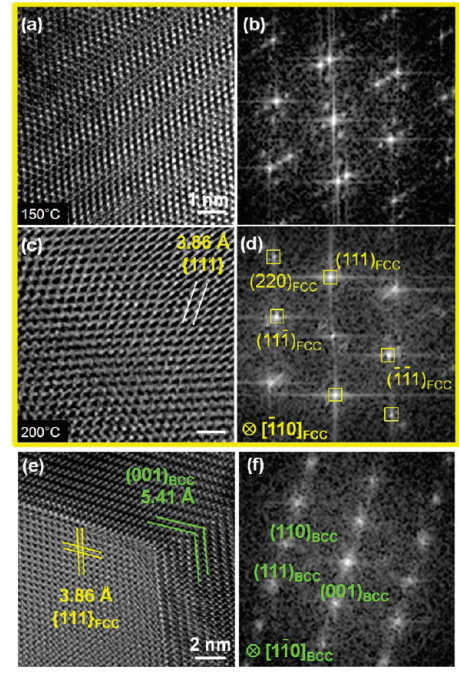

FIGURE 4. (a,c) HRTEM images of the yellow square in Figure 3d at 150 and 200 °C, respectively, and (b,d) the corresponding FFT patterns. The zone axis in panel d is the $[\bar{1}10]_{fcc}$ direction (scale bar, 1 nm; M, monoclinic; white circle, monoclinic spot; yellow square, fcc spot). (e,f) HRTEM image and the corresponding FFT pattern of the white square in Figure 3d, respectively, at 200 °C. The zone axis in panel f is the $[\bar{1}10]_{bcc}$ direction.

DOI: 10.1021/nl102350j | *Nano Lett.* **2010,** *10,* 4501–4504

indicating overlapping of monoclinic and fcc phases. The transition to the bcc phase, rather than to fcc, at the outer boundary region is ascribed to the effect of high compressive stress induced by the large differences in the thermal expansion coefficients between Ag_2Te and the surrounding materials, Pt and sapphire. The thermal stress can be effectively relaxed by volume contraction accompanied by the transition to bcc phase. The bcc phase is formed preferentially along the interfaces where large compressive stress is induced, as predicted by the stress map (Figure 3c).

Figure 4a,b shows magnified HRTEM images of the yellow square region in Figure 3d and its FFT pattern revealing streaky reflections, respectively. The HRTEM image and the FFT pattern of the same region obtained at 200 °C (Figure 4c,d) confirm that the phase transition in this region is completed to fcc phase. The zone axis of the fcc structure is determined to be $[\bar{1}10]_{fcc}$, which used to be the $[1\bar{1}0]_M$ zone axis in the monoclinic structure. Unlike the phase transition of freestanding Ag_2Te NWs, after cooling to RT the fcc phase of the constrained NWs did not completely return to the monoclinic phase. A portion of the fcc phase is retained in coexistence with the monoclinic phase (Supporting Information Figure S6). This might be associated with the different cooling and heating rates used in the present experiments, as they can affect the transition kinetics.

Figure 4e shows an HRTEM image of the white square region outlined in Figure 3d. The HRTEM image was recorded at 200 °C on heating. The measured lattice spacings of 3.86 and 5.41 Å in the boundary and internal regions, respectively, correspond to those of the $\{111\}_{fcc}$ and $(001)_{bcc}$ planes. The FFT pattern obtained from the boundary region is indexed to the $[1\bar{1}0]_{bcc}$ zone axis pattern (Figure 4f). The measured d-spacings were compared to those of potential reaction byproducts such as Pt−Te or Pt−Ag alloys, but none of them match with the measured values, excluding the formation of reaction byproducts.[18] While maintaining 200 °C, we observed the nucleation and growth of barlike bcc phase penetrating into the fcc matrix (Supporting Information Figure S7; this process was recorded in a real-time movie via in situ HRTEM and is presented as Supporting Information.). The secondary nucleation and growth event of a bcc phase inside the fcc matrix is attributed to the increased stress inside the fcc phase upon continuous heating. After the heating−cooling cycle was completed, parts of the bcc as well as the fcc phases remained in coexistence with the monoclinic phase at RT.

In conclusion, we have observed the effect of thermal stress on phase transitions in the constrained Ag_2Te NW, covered with platinum cladding layers, by in situ HRTEM. To alleviate the stress acting on the NW, phase transition from monoclinic to the bcc took place near the interfaces at 150 °C, followed by gradually phase change to the fcc phase inside the NW. Furthermore, we observed in real time that a bcc layer grows within the fcc layer to alleviate the thermal stress at 200 °C. Our in situ HRTEM observation of the constrained phase transition of Ag_2Te NWs illustrates unique phase transition dynamics under compression in atomic detail and also provides direct insight into how nanomaterials would behave when constrained by overlayers in a device.

Acknowledgment. This research was supported by KOSEF through NRL (20090083138), Nano R&D program (20090083221), SRC (2010-0001484), and "Center for Nanostructured Material Technology" under "21st Century Frontier R&D Programs" (2009K000468) of the MEST, Korea. SEM, TEM, and HVEM analyses were performed at KBSI in Daejeon. We thank Professor H. S. Kim for the calculation of thermal stress.

Supporting Information Available. Supplementary figures. A movie showing nucleation and growth of barlike bcc phase penetrating into the fcc matrix. This material is available free of charge via the Internet at http://pubs.acs.org.

REFERENCES AND NOTES

(1) Chen, R.; Xu, D.; Guo, G.; Gui, L. *J. Mater. Chem.* **2002**, *12*, 2435–2438.
(2) Qin, A.; Fang, Y.; Tao, P.; Zhang, J.; Su, C. *Inorg. Chem.* **2007**, *46*, 7403–7409.
(3) Li, F.; Hu, Cz.; Xiong, Y.; Wan, B.; Yan, W.; Zhang, M. *J. Phys. Chem. C* **2008**, *112*, 16130–16133.
(4) Keen, D. A.; Hull, S. *J. Phys.: Condens. Matter* **1998**, *10*, 8217–8234.
(5) Fujikane, M.; Kurosaki, K.; Muta, H.; Yamanaka, S. *J. Alloys Compd.* **2005**, *387*, 297–299.
(6) Banus, M. D.; Finn, M. C. *J. Electrochem. Soc.* **1969**, *116*, 91–94.
(7) Shimojo, F.; Okazaki, H. *J. Phys. Soc. Jpn.* **1992**, *61*, 4465–4473.
(8) Xu, R.; Husmann, A.; Rosenbaum, T. F.; Saboungi, M.-L.; Enderby, J. E.; Littlewood, P. B. *Nature* **1997**, *390*, 57–60.
(9) Hu, J.; Rosenbaum, T. F. *Phys. Rev. Lett.* **2005**, *95*, No. 186603-1−186603-4.
(10) Harpeness, R.; Palchik, O.; Gendanken, A.; Palchik, V.; Amiel, S.; Slifkin, M. A.; Weiss, A. M. *Chem. Mater.* **2002**, *14*, 2094–2102.
(11) Batabyal, S. K.; Vittal, J. J. *Chem. Mater.* **2008**, *20*, 5845–5850.
(12) Simpson, R. E.; Krbal, M.; Fons, P.; Kolobov, A. V.; Tominaga, J.; Uruga, T.; Tanida, H. *Nano Lett.* **2010**, *10*, 414–419.
(13) Mitra, M.; Jung, Y.; Gianola, D. S.; Agarwal, R. *Appl. Phys. Lett.* **2010**, *96*, No. 222111-1−222111-3.
(14) Yoo, Y.; Seo, K.; Han, S.; Varadwaj, K.; Kim, H.; Ryu, J.; Lee, H.; Ahn, J.; Ihee, H.; Kim, B. *Nano Lett.* **2010**, *10*, 432–438.
(15) Sohn, J. I.; Joo, H. J.; Porter, A. E.; Choi, C.-J.; Kim, K.; Kang, D. J.; Welland, M. E. *Nano Lett.* **2007**, *7*, 1570–1574.
(16) Lide, D. R. *Handbook of Chemistry and Physics*; CRC Press: FL, 1995.
(17) Honma, K.; Iida, K. *J. Phys. Soc. Jpn.* **1987**, *56*, 1828–1836.
(18) Okamoto, H. *Desk Handbook: Phase Diagrams for Binary Alloys*; ASM International: Cleveland, OH, 2000.

DOI: 10.1021/nl102350j | *Nano Lett.* **2010,** *10,* 4501–4504